Pharm Res (2012) 29:53–68
DOI 10.1007/s11095-011-0510-x

RESEARCH PAPER

Opsonization, Biodistribution, Cellular Uptake and Apoptosis Study of PEGylated PBCA Nanoparticle as Potential Drug Delivery Carrier

Kiran Ramanlal Chaudhari • Mukesh Ukawala • Arehalli S. Manjappa • Abhinesh Kumar • Piyush Kishor Mundada • Anil Kumar Mishra • Rashi Mathur • Jukka Mönkkönen • Rayasa S. Ramchandra Murthy

Received: 10 March 2011 / Accepted: 10 June 2011 / Published online: 9 July 2011

ABSTRACT

Purpose For nanocarrier-based targeted delivery systems, preventing phagocytosis for prolong circulation half life is a crucial task. PEGylated poly(n-butylcyano acrylate) (PBCA) NP has proven a promising approach for drug delivery, but an easy and reliable method of PEGylation of PBCA has faced a major bottleneck.

Methods PEGylated PBCA NPs containing docetaxel (DTX) by modified anionic polymerization reaction in aqueous acidic media containing amine functional PEG were made as an single step PEGylation method. *In vitro* colloidal stability studies using salt aggregation method and antiopsonization property of prepared NPs using mouse macrophage cell line RAW264 were performed. *In vitro* performance of anticancer activity of prepared formulations was checked on MCF7 cell line. NPs were radiolabeled with 99mTc and intravenously administered to study blood clearance and biodistribution in mice model.

Results These formulations very effectively prevented phagocytosis and found excellent carrier for drug delivery purpose. *In vivo* studies display long circulation half life of PBCA-PEG20 NP in comparison to other formulations tested.

Conclusions The PEGylated PBCA formulation can work as a novel tool for drug delivery which can prevent RES uptake and prolong circulation half life.

KEY WORDS apoptosis · biodistribution · cellular uptake · opsonization · PBCA

ABBREVIATIONS

DTX	docetaxel
EPR	enhanced permeation and retention
NP	nanoparticle
PBCA	poly(n-butylcyano acrylate)
PEG	polyethylene glycol
PMN	polymorphonuclear cells
RES	reticuloendothelial system

INTRODUCTION

In the present scenario, nanocarrier drug delivery systems are emerging as a novel tool to deal with some of the major

Electronic Supplementary Material The online version of this article (doi:10.1007/s11095-011-0510-x) contains supplementary material, which is available to authorized users.

K. R. Chaudhari · M. Ukawala · A. S. Manjappa · A. Kumar · P. K. Mundada
Pharmacy Department
TIFAC Centre of Relevance & Excellence in New Drug Delivery Systems
G.H. Patel Pharmacy Building
The Maharaja Sayajirao University of Baroda
Donor's Plaza, Fatehgunj Vadodara 390002, India

K. R. Chaudhari · J. Mönkkönen
School of Pharmacy, Faculty of Health Sciences
University of Eastern Finland
Kuopio, Finland

K. R. Chaudhari · A. K. Mishra · R. Mathur
Department of Radiopharmaceuticals and Radiation Biology
Institute of Nuclear Medicine and Allied Sciences (INMAS)
Brigadier S. K. Mazumdar Road
Delhi 110054, India

R. S. R. Murthy (✉)
ISF College of Pharmacy
Firozpur G. T. Road
Moga 142001 Punjab, India
e-mail: m_rsr@rediffmail.com
URL: www.isfcp.org

diseases such as cancer. Nanocarrier-based anti-cancer formulations are being introduced into the market with advanced strategic modification and enhanced therapeutic benefit based on localization of these nano-carriers due to enhanced permeation and retention effect (EPR) (1,2). In spite of many reports of proven efficacy of nanocarriers *in vitro* and preclinical studies, very few formulations are successful in clinical assessment. The major limiting factor for nanocarrier's success is NP uptake by reticulo-endothelial system (RES) and subsequent removal of nano-carriers from systemic circulation (1,3). Avoiding RES uptake of nanocarriers by liver and spleen is still a challenge for a formulation scientist.

The macrophage lineage in liver and spleen identifies NPs as a foreign body and remove them to protect the body from infections and hazards. The uptake mechanism is called complement consumption and/or opsonization. As per reported observations, it is now clear that almost all NPs injected without stealth strategy are cleared within few hours from blood circulation by PMN cells of RES (4). It is now widely accepted that the physical and chemical properties of the NPs, including particle size, surface charge and surface hydrophilicity determine biological fate of NPs (5–7). As an anti-opsonization strategy, PEGylation has proven more effective to prevent phagocytosis than all strategies reported, such as dextran conjugation (8), dendrimers (9), polyethylene glycol (PEG) (10) or polyethylene oxide linkage (11). *In vitro* study is very convenient to test the prepared PEGylated nanocarrier systems for phagocytotic activity before going for preclinical studies to reduce time and cost of animal studies. Some reports have demonstrated evaluation of NPs for *in vitro* phagocytosis activity (12,13). Studies such as salt-induced aggregation and serum-induced aggregation studies are popular for investigating opsonization capacity *in vitro*.

The use of cyanoacrylates in drug delivery have been increased due to its inherent properties, such as stability, biodegradability, biocompatibility and targetability (14–16). Several clinical trials have reported good *in vivo* tolerance of NPs prepared from this material (17). Still, the biggest break-through research which gives attention to PBCA as a nanocarrier found it to have predominant activity against resistance cancer with improved efficacy of chemotherapy. The mechanism proved that after adhesion of NPs to cell surface, PBCA's biodegraded products form ion pair with drug and enhance cell internalization without getting efflux by P-glycoprotein (P-gp) transporters, which are responsible for chemotherapeutic resistance formation in cancer (18).

A method of direct NP generation using alkyl cyanoacrylate monomers by *in situ* polymerization was developed and reported by Couvreur *et al.* (19). In spite of good research in this area, there are still several constraints associated with the use of PBCA NP preparation method, e.g., low NP concentration in single batch, particle aggregation, high susceptibility of reaction with presence of impurities, uncertainty and sensitivity of reaction progress and slow process of reinitiation-depolymerization-repolymerization. Toxicity of residual unreacted monomer, stabilizer added previously in monomer (sulphur dioxide, p-toluene sulphonic acid, etc.) and limitation of the number of FDA-approved initiator/additives for monomer are also challenging issues. PEGylation process with easy scalable, batch-to-batch uniformity and better yield without compromising quality still remain a high thrust area of research. The method of redox reaction was good in producing PEGylated PBCA NP, but the increasing number of steps and toxic monomer additives discourage it as a method of choice. BCA polymerization is also suitable for *in situ* conjugation with molecule having basic group, such as -OH, $-NH_2$, which work as an initiator template for polymerization in absence or reduced availability of hydroxyl ion from self-ionization of water (20). There were some attempts made with Methoxy-PEG-OH (21), but no attempts have been reported using PEG-amine, even though it is well known that amine group could work as a stronger initiator of polymerization reaction. Methoxy-PEG-OH has low reactivity of -OH group, which hindered the reaction progress and turned to aggregation due to slow reactivity. With the help of reactive amino-PEG, this problem can be solved, and the single step *in situ* concurrent PEGylation with NP formation could be possible with slight changes in reported methods of PBCA NP formation (22).

In the present work, PEGylated PBCA NPs have been prepared with modified emulsion polymerization method. This method has the unique advantage of single-step *in situ* polymerization, NP formation as well as PEGylation. This new method is also helpful for ligand or antibody conjugation using amine group of PEG derivatives as an initiator of polymerization reaction. The conjugation is also possible with the help of bifunctional PEG, where amine group of PEG is first used as a reaction initiator, and second group could be used for conjugation of antibody or ligand. With varying feed ratio of monomer to PEG, PBCA NPs were prepared with different PEGylation ratio. The prepared NPs were characterized by particle size and zeta potential measurement, FTIR and H^1 NMR for confirmation of polymerization, gel permeation chromatography (GPC) for Mw determination and CryoTEM for surface morphology. Efficacy of PEGylation was confirmed by colloidal stability studies and *in vitro* serum stability studies. *In vitro* phagocytosis studies were performed using mouse macrophage cell line RAW264 to evaluate antiphagocytic potential of prepared

formulations. Utility of these NPs as drug delivery carrier was evaluated using DTX as a model drug. The efficacy of DTX-loaded PBCA NPs was evaluated by cell cytotoxicity, apoptosis, cell cycle analysis and cell uptake by endocytosis in human breast cancer cell line MCF-7. NPs were radiolabeled with ^{99m}Tc, and these radiolabeled complexes were intravenously administered to study blood clearance and biodistribution of NPs in mice model.

MATERIALS AND METHODS

Materials

Butylcyanoacrylate monomer was obtained as a gift sample from Evobond, Tong Shen Enterprise, Taiwan. DTX was obtained as a gift sample from Sun Pharma Advanced Research Company Ltd. (SPARC), Vadodara, India. Methoxy-PEG-amine, PEG bisamine (Mol wt. 3350 Da) and 6-coumarin were purchase from Sigma Aldrich, India. Poloxamer 188 was kindly gifted from BASF, India. HCl, NaOH, SDS, DMF, and DMSO were obtained from S. D. Fine Chemicals, India. MCF-7 cell line was obtained from ECACC (Salisbury, UK), and RAW264 cell line was obtained from ATCC (USA). DMEM 21885, FBS, PBS, Penicillin, streptomycin, tripsin, EDTA and HBSS were purchased from GIBCO, Finland. RPMI 1640 was purchased from Lonza, Finland. 3-(4,5-Dimethylthiazol-2-yl)-2,5-diphenyltetrazolium bromide (MTT) and Propidium Iodide (PI) were purchased from Sigma Chemicals, Finland. All well plates and tissue culture flasks were purchased from NUNC, Finland. Hoechst 33342 and RNAse A were purchage from Invitrogen, Finland. Annexin V-FITC and binding buffer were purchased from Biolegend (UK). Stannous chloride dihydrate ($SnCl_2.2H_2O$) was purchased from Sigma Chemical (St. Louis, MO); sodium pertechnetate, separated by solvent extraction method from molybdenom-99 (99m), was provided by Regional Center for Radiopharmaceutical Division (North Region) Board of Radiation and Isotope Technology (BRIT), India.

Preparation of Nanoparticles

PBCA NPs were prepared by modified anionic polymerization technique described by Mitra and Lin with some modifications (23). Briefly, NPs were prepared in an acidic polymerization medium (pH 1.5–3) containing poloxamer 188 as a stabilizer. Water used was double distilled, filtered through 0.22 μm filter (Millipore, India) and exhibited very low conductivity value. To the prepared aqueous acidic polymerization medium, monomer was added drop-wise with stirring and probe sonicated for 2 min (100 W, 80% amp), followed by constant magnetic stirring at 700 rpm at 4–8°C for 5 h. pH of the polymerization medium was gradually increased up to pH 5 using 0.5 M NaOH and stirred. After 30 min, the NP suspension was neutralized with 0.5 M NaOH, filtered through 0.4 μm filter (Millipore, India), separated by centrifugation (Sigma 3K30, Germany) and lyophilized (Heto Drywinner, Denmark) using trehalose as a cryo-protectant. In the case of DTX and 6-coumarin-loaded PBCA NPs, the respective material was dissolved in monomer before addition into polymerization media. PEGylated PBCA NPs were prepared in similar manner by adding required amount of mPEGamine or PEG bisamine in acidic polymerization medium before addition of monomer.

Precent Drug Entrapment and Loading

Lyophilized PBCA NPs (5 mg) were dissolved in 5 ml acetonitrile. The content of DTX was estimated using reverse phase HPLC using C18 column, mobile phase acetonitrile: water (70:30), 1 ml/min flow rate and 230 nm λ_{max} using ultra-violate detector (Shimadzu, Japan). The % entrapment efficiency was calculated as a ratio of the total entrapped DTX to the total amount of DTX using the below equation:

$$\%\ \text{Entrapment efficiency} = \frac{\text{Amount of Entrapped drug} \times 100}{\text{Total added drug}}$$

Salt- and Serum-Induced Aggregation Studies

Colloidal stability of NPs was tested using salts such as sodium sulphate and calcium chloride, which are well known as colloidal aggregation inducers. NPs were diluted with sodium sulphate (1 M) and calcium chloride (30 mM) solution and kept for fixed time interval under slow stirring, and particle size was monitored. To evaluate serum protein adsorption, NP formulations were mixed with 1% FBS in PBS in 1:10 proportion and kept with slow stirring. After fixed time interval, particle size was measured.

In Vitro Cell Culture Studies

RAW 264 cell line is a mouse macrophage cell line, obtained from ATCC (USA) and maintained in DMEM 21885 GLUTMAX® media along with 10% FBS. MCF-7 cell line is a human breast cancer cell line, obtained from ECACC (Salisbury, UK) and maintained in RPMI 1640 Biowhittaker® media along with 10% FBS. Both cell lines were cultured at 37°C in a 5% CO_2 and 90% RH humidify atmosphere and handled in sterile condition.

Phagocytosis Uptake

1×10^5 RAW 264 cells were seeded on 6-well plate and allowed to attach and grow. After 48 h, cells were incubated with 1 ml, 100 µg/ml 6-coumarin-loaded PBCA NPs as well as PEGylated PBCA NPs, and plates were incubated for 60, 120 and 240 min for phagocytosis. Wells were washed with cold HBSS buffer twice, and each well was treated with sodium azide (10 mM). The cells were harvested using trypsin-EDTA treatment followed by centrifugation and repeated washing in PBS. Samples were kept at 4°C with protection from light, and FACS analysis was performed within 1 h. In FACS analysis, 10,000 cells were counted and analyzed by measuring signal from FITC channel (Canto-II, BD).

Endocytosis by FACS and Microscopy

1×10^5 MCF-7 cells were seeded on 6-well plate and allowed to attach and grow. After 48 h, cells were incubated with 1 ml, 100 µg/ml 6-coumarin-loaded PBCA NPs and PBCA-PEG NPs and incubated for 30 min and 90 min. Cells were washed, harvested and analyzed in FACS (Canto-II, BD) for total amount of NP uptake by 10,000 cells. Same treatment was also performed in micro-slide for purpose of microscopy. After adequate treatment, adherent cells were washed and analyzed under confocal microscope (Carl Zeiss, Axiovert 135M).

Cell Cytotoxicity

MCF-7 cell line was transferred to 96-well plate (5,000 cells/well) and allowed to attach and grow. After 24 h the medium was removed and replaced with 200 µl medium containing DTX solution, DTX-loaded PBCA NPs and PBCA-PEG20 NPs having different concentrations of DTX (0.5, 2, 8 ng/ml). After incubation for 48 h and 72 h, treatment media was removed, and cells were treated with 100 µl (500 µg/ml) of MTT and incubated for 1 h followed by addition of 100 µl SDS solution (20% w/v, Water: DMF in 1:1 ratio, pH 4.7) and allowed the formazan crystals to dissolve. After 24 h, 96-well plate was analyzed at 570 nm wavelength in microplate reader (Victor 1420, PerkinElmer) to determine cell viability.

Cell Cycle Analysis

1×10^5 MCF-7 cells were seeded on 6-well plate and allowed to attach and grow for 24 h. Cells were incubated with 2 ml media containing 5 nM DTX solution, DTX-loaded PBCA NPs and PBCA-PEG20 NPs and incubated. After 24 h, media was removed, cells were washed with PBS and treated with 200 µl of trypsin-EDTA to harvest. Incubation media, washing buffer and trypsin-EDTA treated cell were collected together and centrifuged at 1,500 rpm for 5 min. The cell pellet was washed twice with PBS and centrifuged. Cells were resuspended in 0.86 ml cold PBS and vortexed at slow speed, and 2 ml absolute ethanol was added drop-wise to make final concentration 70% v/v. After 15 min incubation at 4°C, cells were resuspended in 250 µl staining PBS solution composed of RNAse A (0.1 mg/ml), PI (10 µg/ml) and Triton X 100 (0.05%). After incubation for 1 h, cells were analyzed on FACS by recording signal from Texas red channel (Canto-II, BD). Sections were made in the histogram of count *Vs.* intensity to calculate ratio of cells under Go/G1 (2n), S (2n+), G2/M phase (4n) and under apoptosis (2n-).

Apoptosis Using Annexin V-FITC

1×10^5 MCF-7 cells were seeded on 6-well plate and allowed to attach and grow for 24 h. Cells were incubated with 2 ml, containing 1 nM DTX solution, DTX-loaded PBCA NPs and PBCA-PEG20 NPs in media and incubated. After 48 h, cells were harvested and washed. 1×10^5 cells were suspended in 100 µl binding buffer and stained with PI (10 µl, 1 mg/ml) and Annexin-FITC (5 µl), mixed well using vortex shaker and kept for binding. After 30 min another 200 µl binding buffer was added, and suspension was analyzed using FACS at Texas red and FITC channel (Canto-II, BD). The intensity plot of FITC *vs.* Texas Red was sectioned in four quarters to differentiate stained and unstained cells. Based on four quarters, percentage of cells in early apoptotic cells (FITC positive and PI negative), late apoptosis (FITC and PI positive) and necrotic (FITC negative and PI positive) were calculated.

Pharmacokinetic Studies by Radiolabeling Technique

The formulations were radiolabeled using technetium (^{99m}Tc) by earlier reported method (24,25). Technetium in sodium pertechnetate was reduced in the acidic condition in the presence of stannous chloride. Technetium is reduced in the presence of NPs and formed the NPs tagged with technetium.

Labeling Efficiency

The radiolabeling efficiency of the formulations was estimated using thin layer chromatography (TLC). Silica gel-coated fiberglass sheets (Gelman Sciences, MI) were used as stationary phase, while solvent system consisting of acetone and pyridine: acetic acid: water (3:5:1.5 v/v) was

used as mobile phase (26,27). The unlabeled technetium has R_f value of nearly 1, while labeled NPs retained an R_f near to zero. Thus, the ratios of radioactivity in the top one third to lower two thirds of the TLC were considered as the percentage labeling efficiency.

Biodistribution Studies

Animal experiments were approved by Committee for the Purpose of Control and Supervision of Experiments on Animals (CPCSEA), Ministry of Social Justice and Empowerment, Government of India, New Delhi, India. Swiss mice (aged 6 to 8 weeks), having weight between 20 and 25 g, with tumor (1 to 1.5 cm, ehrlich ascites tumor) were selected for the study. Each formulation and time point was tested in triplicate. One hundred μL radiolabeled formulations were injected in tail vein of the mice. Mice were sacrificed by cervical dislocation, and tissues/organs (tumor, liver, spleen, lungs and blood) were isolated. All collected tissues/organs were estimated for presence of radioactivity using gamma scintillation counter and calculated as a fraction of total dose injected using below equation (25,28):

$$\%\ Radioactivity\ per\ g\ of\ tissue = \frac{Counts\ in\ sample \times 100}{Wt\ of\ sample \times Total\ counts\ injected}$$

RESULTS

PBCA NPs prepared with 0.5–1.0% v/v of monomer concentration showed particle size below 100 nm. With increase in concentration from 1.0% to 2.5% v/v, a rapid increase in particle size was observed with visible aggregation above 1.0% v/v. Also, at higher concentration of monomer (>1.0% v/v), polydispersibility index (PDI) increased, representing wider particle size distribution. Hence, 1% v/v was selected as optimum monomer conc. DTX solubility in monomer was found to be an important formulation variable in achieving NPs with desired entrapment efficiency and particle size. All prepared NP formulations were characterized for particle size, zeta potential and cryoTEM, and respective reports are shown in Figs. 1 and 2. The PBCA NP formation as well as PEGylation reaction were confirmed by FTIR, H^1 NMR and GPC. The reports are shown in Fig. S-1, S-2 and S-3, respectively, in Electronic Supplementary Material (ESM).

DTX conc. was gradually increased in monomer, and its effect on entrapment efficiency and particle size was studied. Maximum DTX solubility in monomer was found to be 7% w/v. DTX conc. above 5% w/v showed no significant/appreciable increase in entrapment efficiency, possibly due to leaching of drug before micellar formation causing drug precipitation. However, DTX conc. below 5% w/v showed no evidence of precipitation with maximum entrapment of about 77.38% w/w with drug loading of 3.69% w/w because of re-entry of drug in micellar structure after leaching from monomer droplets (Fig. 3).

The NP formation is directed by micelle formation, which is a self-stabilized system without any need of surfactant. After NP formation, surface of NP remains covered by grafted PEG, which prevents aggregation and stabilized particle in colloidal form. But use of low concentration of surfactant (poloxamer 188, 0.1% w/v) gave good reconstitution ability to formulation after lyophilization. For this reason, 0.1% w/v poloxamer 188 was used with PEG. In batches without PEGylation, addition of 0.5% w/v surfactant was found satisfactory. PBCA NPs were found to have zeta potential well toward the negative side (−17.64 mV). With the addition of 20 mol% mPEG, negativity of the nanoparticles was reduced to −8.26 mV. However, in the case of PEG-bisamine, the zeta potential was found to be still lower (−4.38 mV) (Table I, Fig. 1). The *in vitro* drug release profile from the lyophilized NPs in phosphate buffer (pH 7.4) containing 10% ethanol and 0.5% v/v tween 80 was sustained and biphasic (Fig. 4). The initial burst release was due to the release of drug located on and near the surface of the NPs. In the second phase, the release was slower and controlled by diffusion rate of drug across the polymer matrix and polymer erosion. The % release of 6-coumarin-loaded NP formulations was performed, and the % release after 6 h was tabulated (Table S-1 in ESM). The % release of 6-coumarin was below 5% w/v, which proved suitability of this marker to use for flow-cytometric-based analysis.

Comparative evaluation of aggregation resistance property of PEGylated and non-PEGylated NPs was performed using salt-induced aggregation and serum-induced aggregation technique. Results showed that out of all formulations PBCA-PEG20 NPs and PBCA-PEG-PBCA NPs displayed exceptionally high resistance to aggregation (Fig. 5a and b). Results of serum-induced aggregation showed no significant increase in particle size with PBCA-PEG20 NPs and PBCA-PEG-PBCA NPs, and PBCA-PEG10 NPs showed slight increase with time, while PBCA-PEG5 and PBCA NPs displayed dramatic increase in particle size with time (Fig. 5c).

PBCA-PEG20 NP showed tremendous protein repellent property under *in vitro* condition, which indicated its ability to prolong circulation half-life *in-vivo*. Further, to confirm *in vitro* antiopsonization activity, phagocytic study was performed with mouse macrophage cell line RAW264. Among the tested formulations, PBCA-PEG20 showed least phagocytic uptake, and the decrease was about seven times in

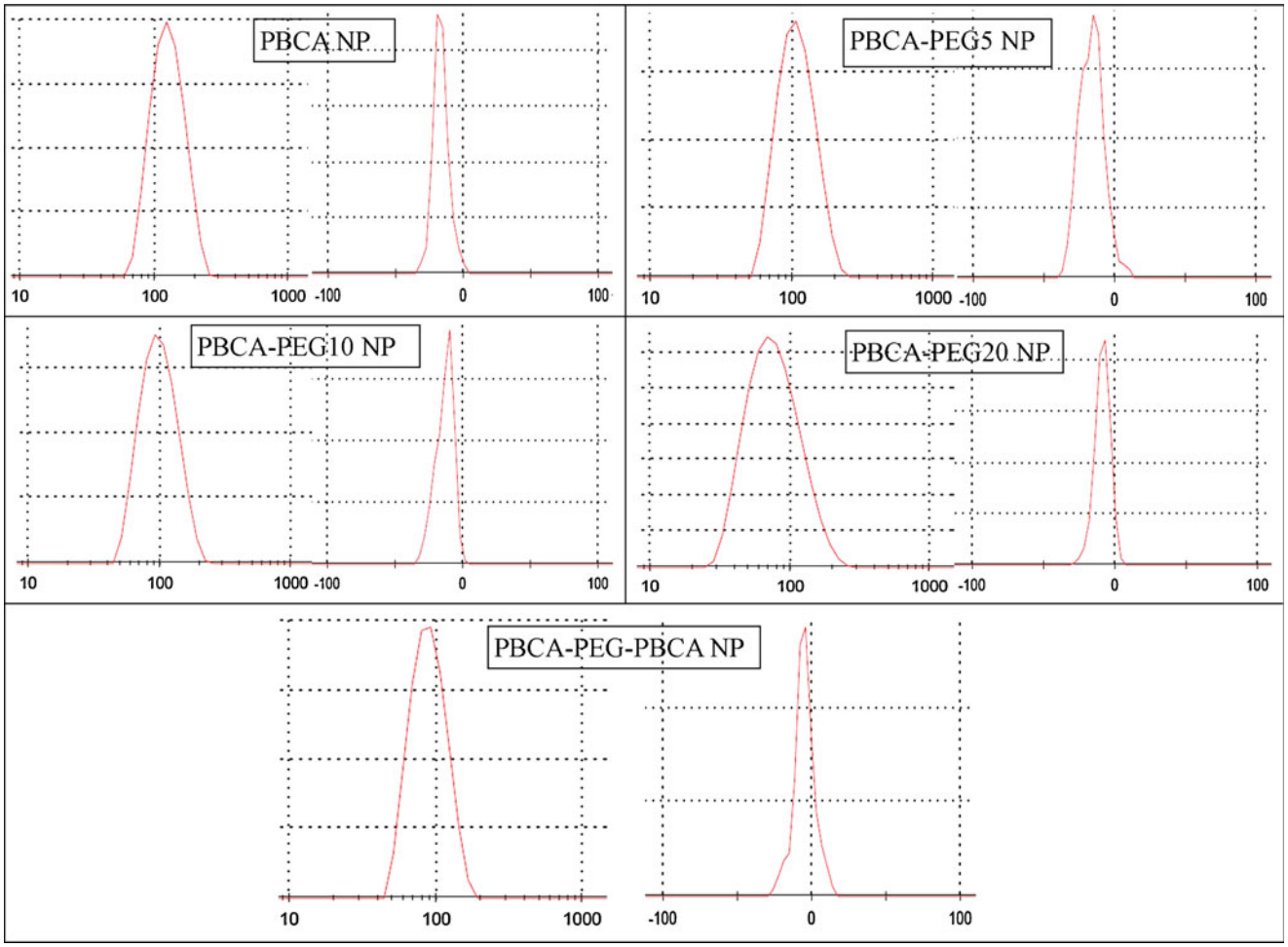

Fig. 1 Particle size analysis and zeta potential measurement using Malvern Zetasizer.

comparison to PBCA NP. PBCA-PEG10 and PEG-PBCA-PEG also displayed moderate resistance to phagocytosis as the cellular uptake was about three times less than PBCA NP. Comparing PBCA-PEG formulations containing varied concentration of PEG (5%, 10% and 20%), phagocytic uptake decreased drastically with increase in PEG concentration from 5% to 10%, while further increase to 20% showed a moderate influence (Fig. 6), which may be due to saturation in the phagocytic inhibition process. Phagocytosis increased modestly with time in all formulations. At 240 min time point, all histograms showed split distribution as a sign of NP degradation in macrophage as florescence intensity started diminishing intracellularly after phagocytosis (Fig. 7). Phagocytic uptake was also observed under confocal microscope after incubation of 6-coumarin-loaded PBCA NP and PBCA-PEG20 NP in RAW 264 cell line. Cells' nuclei were stained with Hoechst 33342. Results showed significant increase in cellular up of PBCA NP in comparison to PBCA-PEG20 NP (Fig. 8). In MCF-7 cells, PBCA-PEG20 NP showed enhanced uptake (55.2% at 30 min) in comparison to PBCA NP after 30 min incubation. This difference of uptake increased with time, which can be inferred from results at 90 min incubation (Fig. 9).

MTT assay is a widespread method to assess cell cytotoxicity. MTT dye is reduced by mitochondrial dehydrogenases in live cells and produces blue-magenta-colored formazan precipitate whose concentration can be correlated with the number of intact alive cells (29). Blank PBCA NP (without DTX) was also evaluated for cytotoxicity evaluation and showed no significant toxicity (Fig. 10). Cytotoxicity curve and IC 50 value were determined for DTX, PBCA NP and PBCA-PEG20 NP. Results showed that PBCA-PEG20 NPs reduce IC50 value approximately 2-fold at 48 h time point and 3-fold at 72 h time point (Fig. 11). PBCA NP also displayed reduction in IC50 value in comparison to DTX solution. At 72 h, IC50 value for PBCA NP reduced approximately half in comparison to DTX, but at 24 h the difference was less significant than PBCA-PEG20 NP.

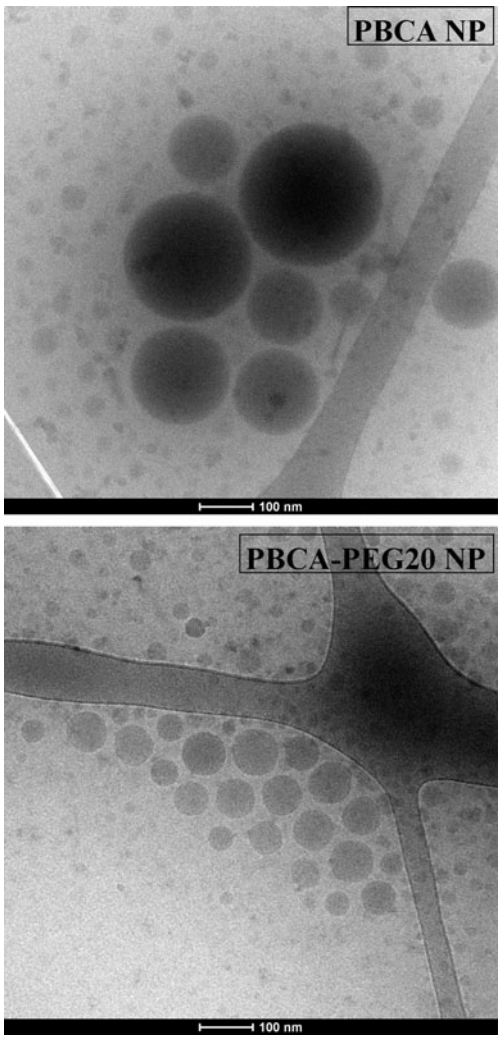

Fig. 2 Cryo Transmission Electron Microscopic (CryoTEM) images of PBCA NP and PBCA-PEG20 NP.

Apoptotic activity always routed with translocation of phosphatidylserine from cytosol to cell membrane. Phosphatidylserine specifically binds with FITC-tagged Annexin V and can be accurately estimated quantitatively by FACS as a very specific apoptotic marker (30). Apoptotic activity of formulations was estimated in cancerous cell line MCF-7 stained previously by Annexin V-FITC and PI staining, after treatment with formulations. In Fig. 12, upper left square among four squares shows proapoptotic cells, upper right shows late apoptotic cells, lower left shows normal live cells and lower right shows necrotic cells. From results, it can be concluded that PBCA-PEG20 NP (6.55+27.48%) shows better apoptotic effect in comparison to PBCA NP (3.97%+23.03%), DTX (2.14%+14.72%) and control group (0.42%+3.36%) (Fig. 12). FACS report also displayed amount of proapoptotic, late apoptotic, necrotic and living cells in each treatment group. Control treatment group demonstrated negligible presence of apoptosis and necrotic cells.

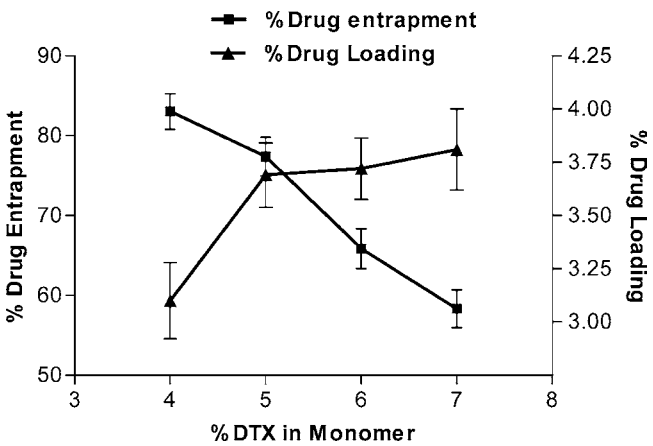

Fig. 3 Effect of DTX concentration in monomer (BCA) on % drug entrapment and % drug loading efficiency.

Analysis of a population of cells in each replication state can be achieved by fluorescence labeling of the nuclei with PI staining and then estimation of DNA content by FACS analysis (31). Cell cycle analysis has been performed by FACS using PI staining in MCF-7 cell line after treatment with formulations. Figure 13a presents cell cycle distribution of control group with 62.99% cells in G0/G1 phase, 11.94% in S phase, 23.84% cells in G2/M and only 1.23% cells in Sub G0/G1 phase. After treatment with DTX the cell cycle arrested and majority of cells were at G2/M check point with 5.63% cells at Sub G0/G1 phase (Fig. 13b). After treatment with PBCA NP, report displayed similar blockage at G2/M check point as with DTX treatment, but more cells (12.19%) at Sub G0/G1 phase due to apoptosis (Fig. 13c). After treatment with PBCA-PEG20, blockage at G0/M check point remained stalemate as DTX and PBCA treatment with significant increase in amount of apoptotic cells at Sub G0/G1 phase, which signified better efficacy of PBCA-PEG20 as a carrier for DTX among tested formulations (Fig. 13d).

The prepared ^{99m}Tc-NPs complex was tested for labeling efficiency using ITLC method. Both PBCA NP (98.6%) and PBCA-PEG20 NP (98.2%) demonstrated high labeling efficacy as more than 98% activity found at base (lower two thirds). From the results of blood to liver NP distribution ratio, significant change was observed in distribution of both NP formulations in blood and liver compartment, which further increased with time (Table II). At 1 h time point, distribution ratio of PBCA-PEG20 NP was 3-fold higher than distribution ratio of PBCA NP. At 4 h time point, the distribution ratio increased to 4-fold, and even at 24 h time point it increased considerably to more than 6-fold. The tumor retention in comparison to liver for PBCA-PEG20 NP was significantly higher (315%) than for PBCA NP after 24 h. At 1 h (168%) and 4 h (239%) the retention was also relatively high. Results clearly showed that PBCA-PEG20 NP demonstrated prolonged circulation time and better tumor retention.

Table I Physicochemical Characterization of PBCA NP and PEGylated PBCA NP

Formulation	% Molar conc of PEG added	Content of PEG obtain (% molar)	Particle size	Zeta potential	% Drug Entrapment	% Drug loading	Mw by GPC (Dalton)
PBCA	0	–	118 ± 6.35	−17.64 ± 2.21	43.07 ± 2.43	2.05 ± 0.11	3126
PBCA-PEG5	5	4.76 ± 1.54	102 ± 7.82	−15.41 ± 1.69	51.75 ± 3.42	2.46 ± 0.13	5948
PBCA-PEG10	10	9.13 ± 1.68	89 ± 6.81	−13.53 ± 1.53	64.58 ± 2.86	3.08 ± 0.24	6173
PBCA-PEG20	20	17.65 ± 2.17	81 ± 5.63	−8.26 ± 1.26	77.38 ± 3.20	3.69 ± 0.15	5845
PBCA-PEG-PBCA	50	41.52 ± 4.75	83 ± 7.04	−4.38 ± 1.08	67.60 ± 3.56	3.22 ± 0.17	8462

DISCUSSION

The NP formation was prepared here by micellar emulsification process. After sonication the size of monomer globules reduced to 1 to 10 µm range and were stable due to the presence of surfactant and/or PEG in the system (Fig. 14b). The reactive amine group of PEG-amine available at the surface of the globule initiates and allows propagating the polymerization reaction with time (Figs. 14 and 15). After growing up to an oligomer, some trace amount of inhibitor (ex. sulphur dioxide, methansulphonic acid, *p*-toluene sulphonic acid and cynoacrylic acid, usually added in monomer to reduce reactivity of monomer for stability and easy handling purpose) present in monomer droplet hindered propagation of reaction to form long chain polymer (32). The oligomer has PEG at one end and small oligomeric hydrophobic polymer chain, which behaves like amphiphiles. Due to solubility in aqueous phase, oligomers start diffusing in aqueous phase from monomer droplets. As time progress, the concentration of oligomer increases sharply due to which it cross critical micellar concentration (CMC) and starts forming micelles (Fig. 14c). Monomer solubility increases in aqueous phase in presence of surfactant and/or PEG, so monomers start diffusing out of monomer droplets and make micelles richer with monomers. In absence of acidic inhibitors in micellar core, the oligomers start polymerization again by repolymerization

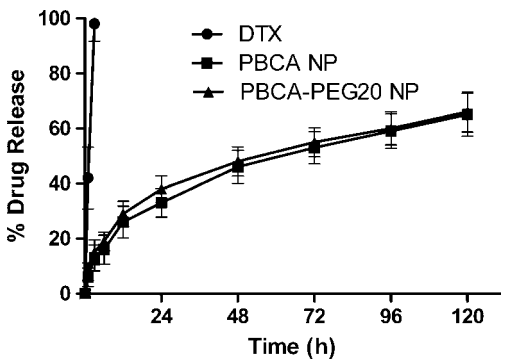

Fig. 4 *In vitro* drug release study for DTX solution, PBCA NP and PBCA-PEG20 NP formulations in phosphate-buffered saline (pH 7.4) containing 0.5% v/v tween 80.

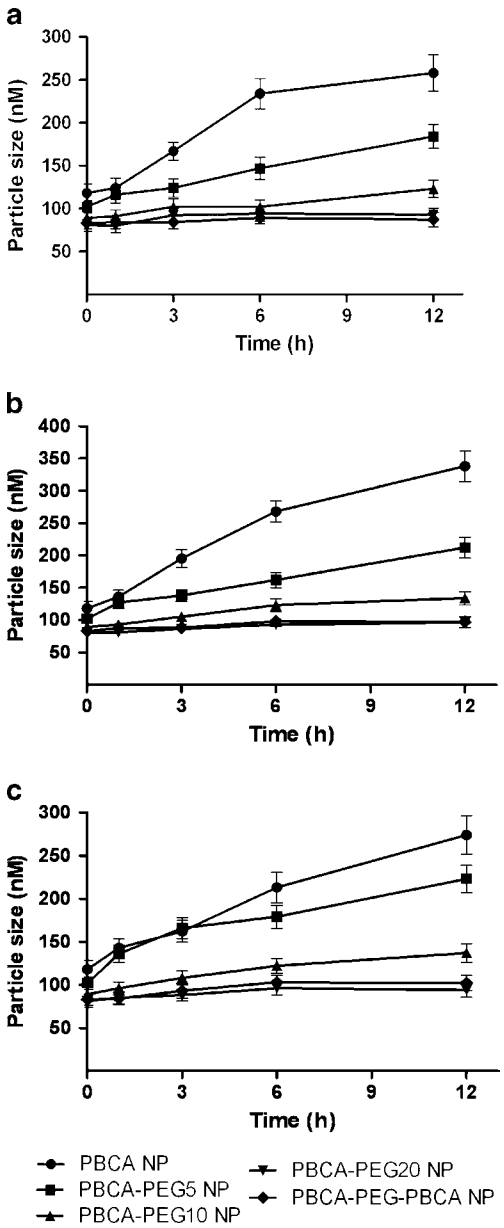

Fig. 5 Colloidal stability study using salt-induced aggregation using (**a**) Na_2SO_4 and (**b**) $CaCl_2$. (**c**) Serum stability study of NP formulations in phosphate-buffered saline (pH 7.4) containing 1% FBS.

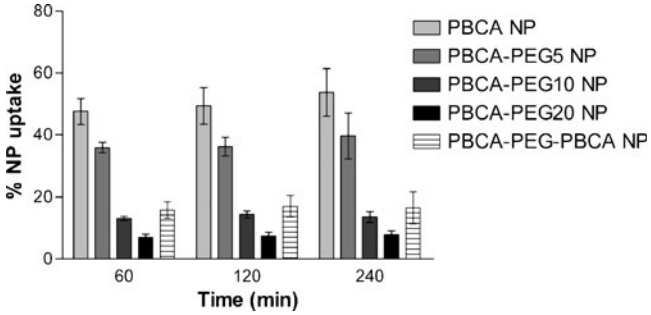

Fig. 6 Phagocytic uptake of coumarin6-loaded NP formulations by mouse macrophage cell line RAW 264 after incubation for 60, 120 and 240 min using FACS as estimation technique.

process (Fig. 15). The diffusion of monomer continues with time, and oligomers then turn to long chain polymer. The micelles increase in size with time as polymer chain length increases and lose their micellar properties, which turns them to NPs (Fig. 14d). The fact that NP formation begins concurrently with the oligomer formation rather than high Mw polymer is investigated by N. Behan *et al.* (32). Because of amphiphilic nature of oligomer, the particle formation is very uniform and prevents agglomerate formation which is otherwise found with unPEGylated PBCA NP. After reduction in monomer availability the polymers in NP start reinitiation-depolymerization-repolymerization process (RDRP) to equilibrate critical degree of polymerization (CDP) of all polymer chains (32,33). The process of RDRP, which is the phenomenon of molecular weight shifting, explains why in PBCA NP all polymers have narrow Mw distribution even though very fast polymerization occurs at higher pH (32). RDRP is a very important process which consumes unused monomer in NP and thereby reduces toxicity and chance of aggregation of NP. Therefore, the PBCA polymer chain is described as 'truly alive' which reactivates at any time in response to any change in surrounding environment (34). This process takes longer time at low pH because of low reaction rate in absence of basic ions. This rate can be largely affected by presence of OH ion and can be increased with increasing pH of the medium up to pH 5 to reduce time needed for completion of reaction.

DTX is very hydrophobic in nature and soluble in momoner (saturated solubility 7%). The amount of docetaxel used for NP formulation was 5% w/v, slightly less than saturated solubility. After addition of monomer into the medium followed by sonication, NP formation starts with micelles formation. But because of constant consumption of monomer, the content of DTX in monomer exceeded saturation solubility limit and started diffusing from monomer droplets. Due to hydrophobic nature of DTX, it diffuses in micelles and gets entrapped in micellar core (Fig. 14d). As time progress, more and more DTX molecules diffuse from monomer droplets and get entrap-

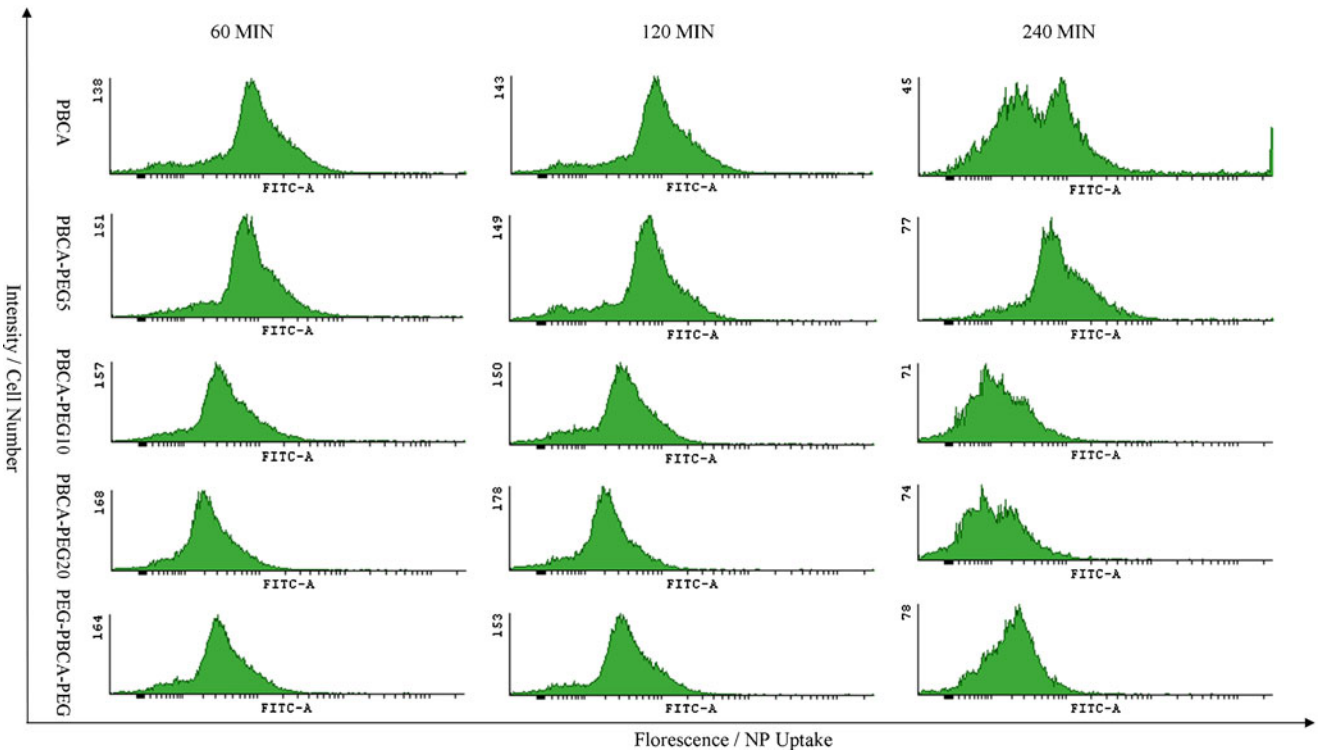

Fig. 7 Phagocytic uptake Histograms of coumarin6-loaded NP formulations by mouse macrophage cell line RAW 264 after incubation for 60, 120 and 240 min using FACS as estimation technique.

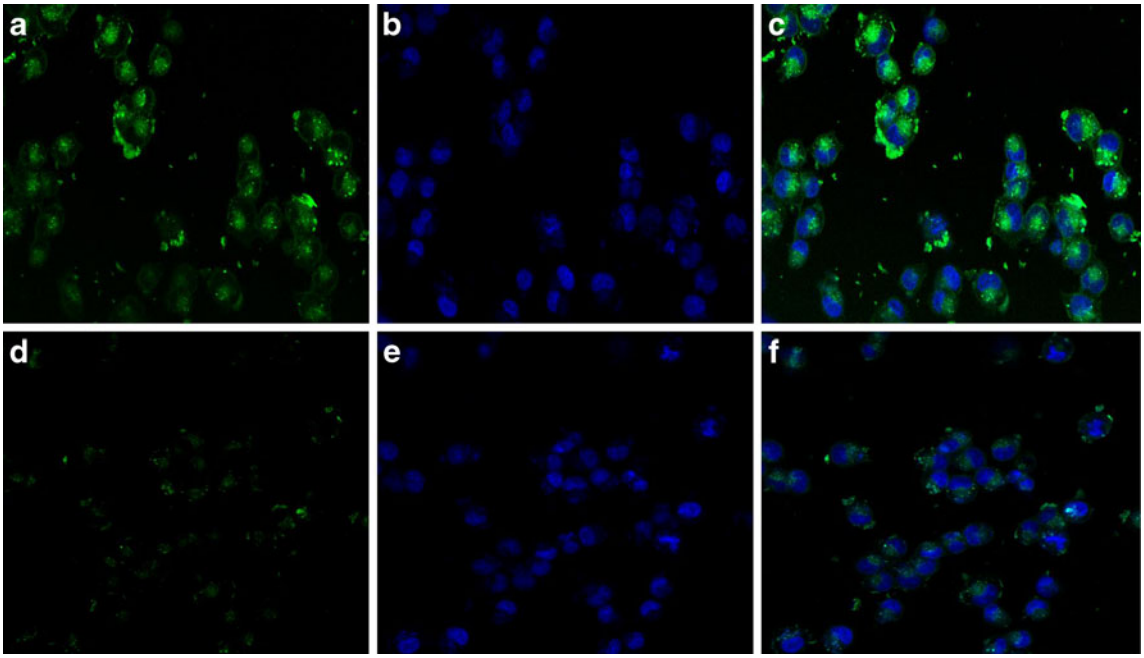

Fig. 8 Microscopic evaluation of phagocytic uptakes of PBCA NP and PBCA-PEG20 NP using confocal microscope. (**a**–**c**) PBCA NP; (**d**–**f**) PBCA-PEG20 NP; (**a** and **d**) coumarin6-loaded NP uptake; (**b** and **e**) nucleus stained using Hoechst 33342; (**c** and **f**) overlapping images.

ped in inner core of micelles. Polymer chain length and size of NPs increased with time, and the DTX molecule got entrapped permanently in polymer matrix of NPs with no evidence of unentrapped DTX precipitate.

At low monomer concentrations (<1% v/v), the amount of monomer molecules available for polymerization is very limited, which restricts the size of the NPs below 100 nm. Higher availability of monomer increases reaction rate of polymerization and increases overall particle size, but with limited availability of initiator and susceptible side reaction increase possibility of aggregate formation. At high monomer concentration, the primary particles formed undergo further polymerization leading to overall increase in particle size. The ratio of PEGylation can be controlled by adjusting feed ratio of PEG to monomer. Ratio of monomer to PEG is very crucial in the case of bisamine-PEG for type of block formed. At low PEG concentration (<50% of monomer conc.) it forms tri-block, while at high concentration (>50% of monomer conc) it preferably forms diblock copolymer (21).

The negative zeta potential of PBCA NP is largely contributed by hydroxyl ions and may be carbonyl group of

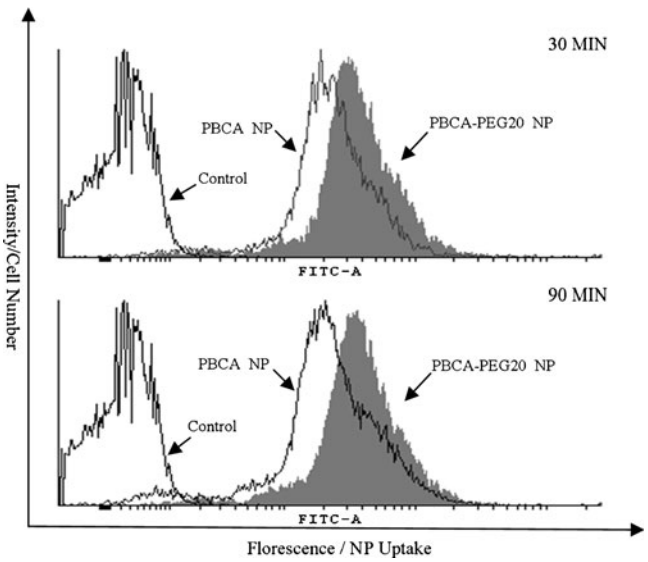

Fig. 9 Endocytic uptake of coumarin6-loaded PBCA NP and PBCA-PEG20 NP in human breast cancer cell line MCF7 after incubation for 30 min and 90 min using FACS as estimation technique.

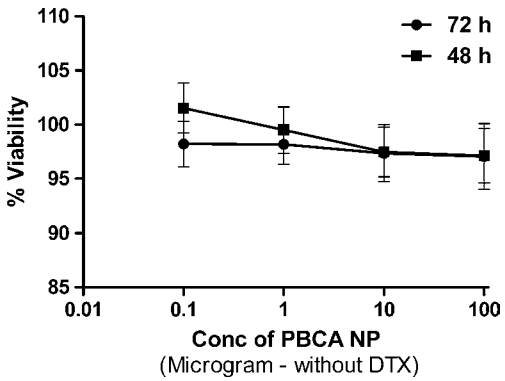

Fig. 10 Cytotoxicity of PBCA NP without DTX in MCF-7 cell line at 48 h and 72 h time point.

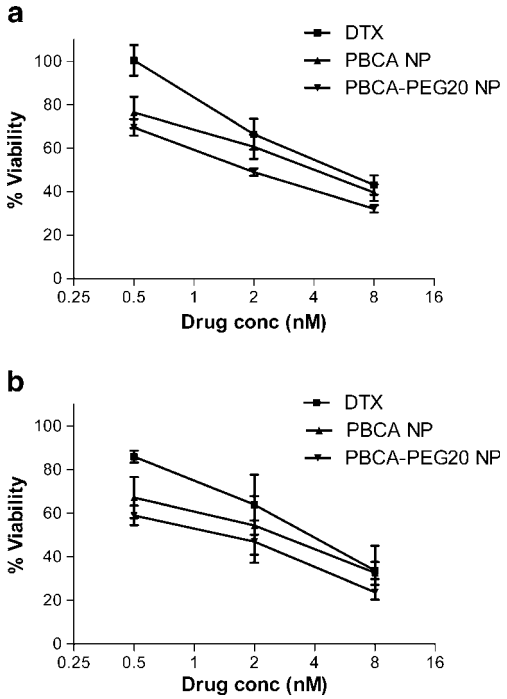

Fig. 11 Cytotoxicity study of DTX solution, PBCA NP and PBCA-PEG20 NP in MCF7 cell line after 48 h (**a**) and 72 h (**b**) using MTT assay.

polymer present on surface of NPs. With the addition of mPEG, zeta potential starts diminishing due to replacement of –OH group with PEG and shields other function group on surface of NPs. With triblock formation the zeta potential was reduced, which gave strong speculation about flower configuration (Fig. 15) of triblock where PEG grafts give non-flexible tight shielding on surface, which effectively hides negativity and surface is largely exposed with bended PEG chain which is electro-neutral in nature.

In biodegradable matrix systems, the drug release rate depends on the molecular weight and hydrophobicity of the polymer. Report on *in vitro* study showed that longer hydrophobic alkyl side chains would effectively shield against the hydroxyl ions to attack the ester groups of PBCA polymer and thus decrease the hydrolysis rate of PBCA. In addition, presence of larger quantity of hydrophobic drugs like DTX would contribute to increased hydrophobicity of the polymer matrix resulting in the increased barrier for water and hydroxyl ions to cause degradation of PBCA polymer (35). Therefore, the relative drug release rate decreases with increasing DTX content in NPs. The slow release of DTX also increases speculation of chemical bonding or interaction between groups of DTX with polymer matrix of NPs. This observation also supports

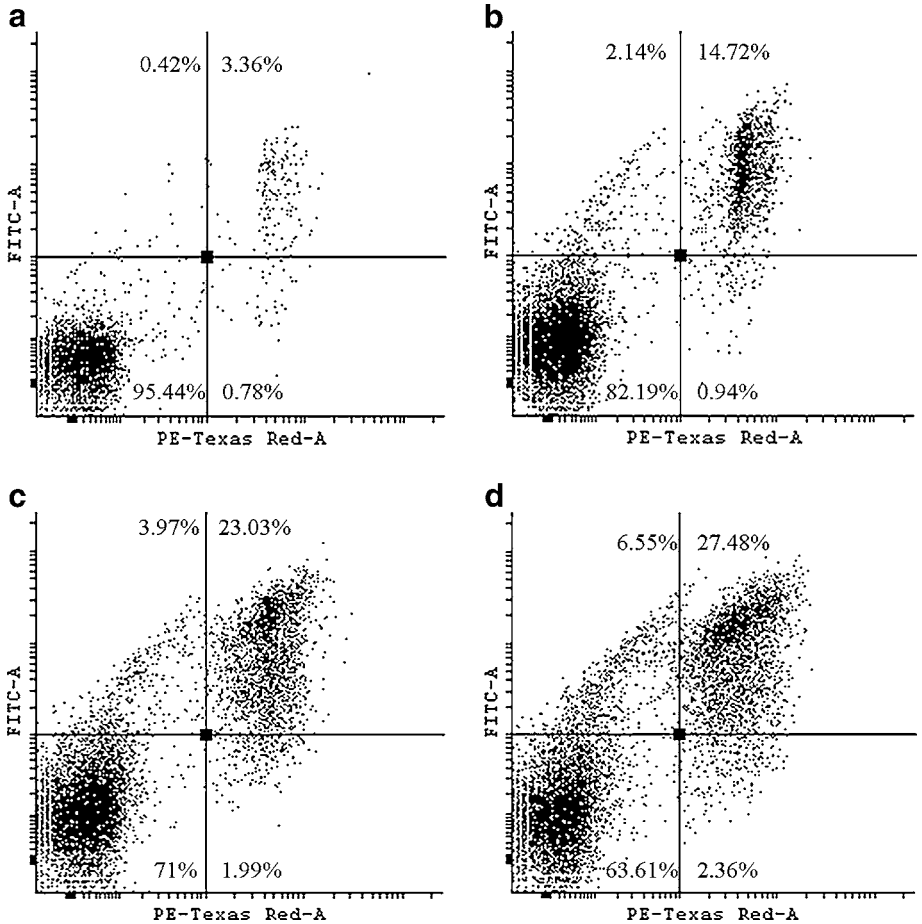

Fig. 12 Appotosis estimation in human cancer cell line MCF7 after treatment of Control (PBS), DTX solution, PBCA NP and PBCA-PEG20 NP by Annexin V-FITC & PI staining using FACS technique.

	G0/G1	S	G2/M	Sub G0/G1
CONTROL	62.99 ± 2.14%	11.94 ± 0.84%	23.84 ± 1.35%	1.23 ± 0.42%
DTX	24.03 ± 1.62%	10.35 ± 0.69%	59.99 ± 2.37%	5.63 ± 0.71%
PBCA NP	27.67 ± 1.38%	11.49 ± 0.74%	48.65 ± 1.92%	12.19 ± 0.78%
PBCA-PEG20 NP	22.36 ± 1.63%	10.65 ± 0.83%	48.55 ± 1.63%	18.44 ± 1.43%

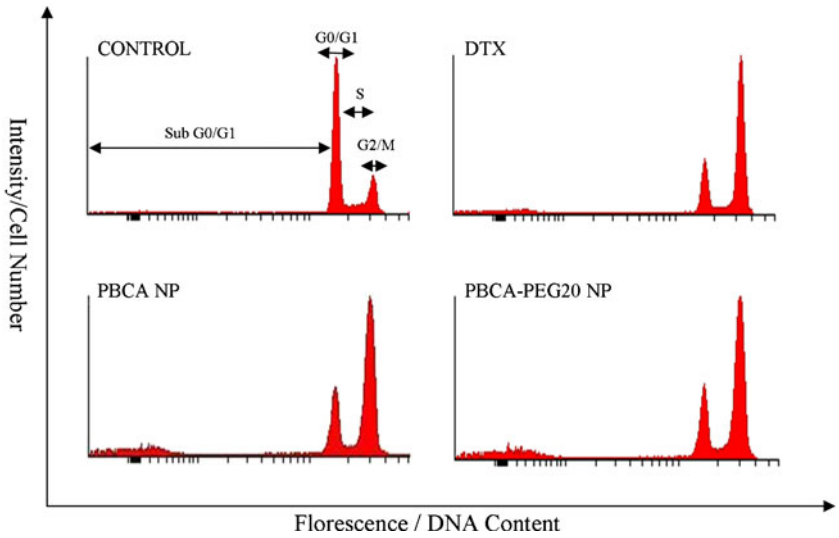

Fig. 13 Cell cycle analysis in human cancer cell line MCF7 after treatment of Control (PBS), DTX solution, PBCA NP and PBCA-PEG20 NP by PI staining using FACS technique.

with earlier report that amine group of drug may also work as an initiator and bond chemically with PBCA polymer, which stops drug release by diffusion (35).

NPs with PEG grafting have very slight increase in particle size, while non-PEGylated NPs show drastic rise in particle size, which shows liability of NPs for aggregation. The process of phagocytosis initiated with adsorption of serum protein, which enhanced recognition by macrophage cells. It is well established that phagocytosis is a cellular phenomenon initiated by the attachment of the foreign particles on to the surface receptors of the phagocytic cells (36). This attachment can be facilitated by the absorption of plasma proteins (opsonins) to the particle surface (37,38). Muller and co-workers illustrated that PLL*g*- PEG-coated PLGA microspheres showed low protein adsorption compared to uncoated PLGA microspheres (39). Hence, adsorption of protein is an important parameter to evaluate *in vitro* and to predict stability of NPs *in vivo*. After protein adsorption, size of NPs increased, and it became highly prone to aggregation in serum-containing media. The adsorption of serum protein was assisted by electrostatic and hydrophobic interaction of protein with NP surface. With protein adsorption, size of NP might increased and result in aggregation. NPs with PEG graft at surface provide protein repellent property and offer no hydrophobic or electrostatic interaction for protein; thus, colloidal solution remains stable for a long time.

A process of phagocytosis commences by two ways: first is by protein adsorption and second is by secretion of pro-inflammatory cytokines. Kanchan *et al.* demonstrated that process of phagocytosis could exert *in vitro* condition using macrophage cell line. After incubation of NP with macrophage cell line, secretion level of IFN-c and IL-4 increases (40,41). Rothen-Rutishauser *et al.* found similar result as 2–3-fold increase of IFN-c when *in vitro* macrophage cell line incubated with NP (42). A few studies also reported *in vitro* macrophage culture to evaluate phagocytosis of PEGylated NPs and found 3-fold reduction of cellular uptake with PEGylated NP in comparison to non-PEGylated NP (12).

Macrophage lineage of liver and spleen is associated with opsonization and subsequent removal of harmful foreign body from blood. This condition can be simulated *in vitro*

Table II Ratio of Radioactivity (^{99m}Tc-NP Complex) for Blood to Liver and Tumor to Liver Per Gram of Organ/Tissue

	Formulation	Time		
		1 h	4 h	24 h
Blood to liver ratio	PBCA NP	0.50	0.371	0.305
	PBCA-PEG20 NP	1.588	1.50	1.938
Tumor to liver ratio	PBCA NP	0.0174	0.0381	0.139
	PBCA-PEG20 NP	0.0294	0.091	0.438

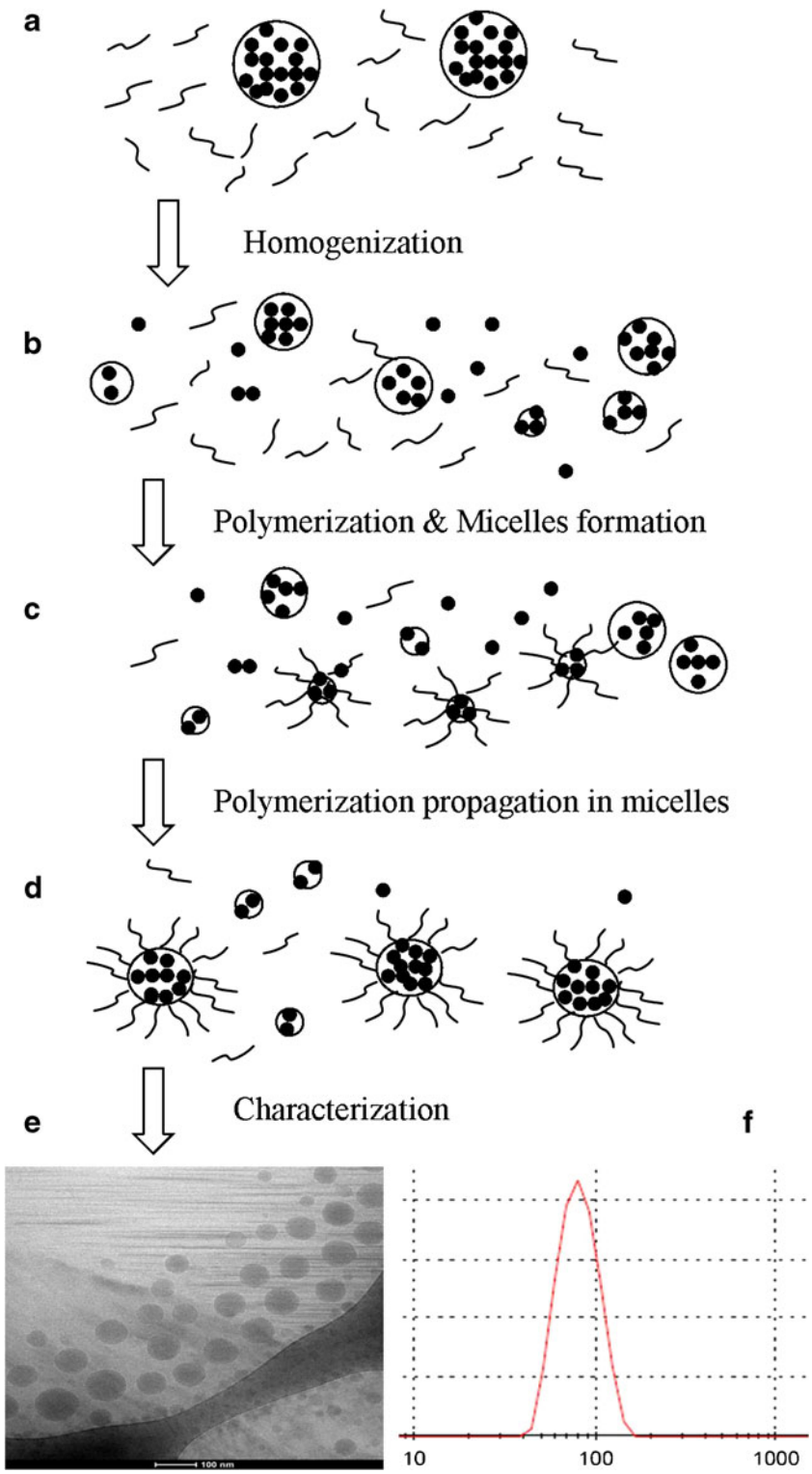

Fig. 14 PEGylated PBCA NP formation, drug entrapment mechanism (**a**–**d**) and characterization by cryoTEM (**e**) and particle size analysis (**f**).

using RAW 264 cell line, which is basically macrophage cell line, demonstrating opsonization and/or compliment consumption characteristic as well. This tool was selected for estimation purpose of antiopsonization liability of NP and quantitative comparison among different NPs uptake with time. All PBCA NPs were prepared with entrapped florescence dye 6-coumarin as a marker to estimate amount of NPs by cells using very specific and selective florescence-assisted cell sorting (FACS) technique. Uptakes of NPs were also confirmed by microscopy using

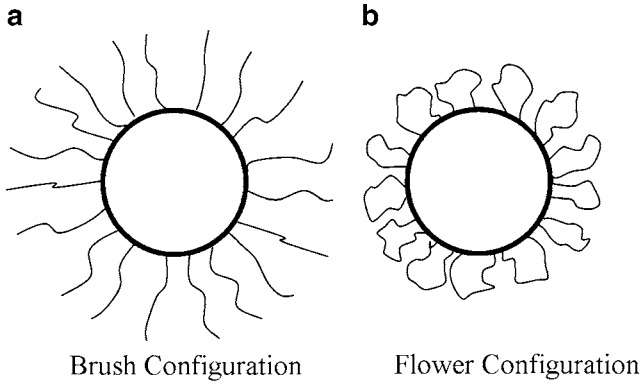

Fig. 15 Orientation of PEG chain in PEGylated PBCA NP: (**a**) brush configuration; (**b**) flower configuration.

confocal microscope (Carl Zeiss, Axiovert 135M), which demonstrated similar observations supporting our findings using FACS technique.

In this study, macrophage cell line RAW 264 was used, which is mouse macrophage cell line and widely used for *in vitro* phagocytosis studies of NPs (43). We have evaluated comparative cellular uptake of NPs at three different time points to determine phagocytosis kinetics where it was found that phagocytosis increases in a time-dependent manner. Uptake was found to increase with time, but decreases with increase in PEG density. These results are in relevance with earlier reports (5,38). However, in the case of PBCA-PEG-PBCA, cellular uptake is high in comparison to PBCA-PEG20, which has lesser PEG density. This observation demonstrates the effect of orientation of PEG in NP on cellular uptake. In the case of PBCA-PEG20, PEG has possibly oriented tangentially, making 'brush configuration', while in the case of PBCA-PEG-PBCA, PEG has oriented in circular bended U shape, making 'flower configuration', as shown in Fig. 15. It is well established that steric repulsion to serum protein depends of 'dynamic hydrophilic cloud', chain length and chain flexibility (44,45). In both configurations, it can be inferred that 'brush configuration' displays a clear advantage, as more dynamic hydrophilic cloud volume, chain length and chain flexibility. In 'flower configuration', both ends of PEG are in bound form which reduces, size of hydrophilic cloud, chain length and chain flexibility in comparison to brush configuration (22). As a result, PBCA-PEG-PBCA has more PEG content and still has less resistance to phagocytosis. At 240 min, the cellular uptake histograms start splitting, which gives indication of decrease in fluorescence intensity which may be due to 6-coumarin degradation along with NPs. NP uptake by cancerous cell line usually occurs by endocytosis process. It can be speculated that the enhanced uptake is a consequence of better interaction of PEG-grafted NP with cell membrane resulting in higher endocytosis uptake and/or higher residence time of PEG-grafted NP in intracellular domain.

Radiolabeling of drugs and nanocarrier systems was performed to study their organ distribution pattern and their fate *in vivo*. We have already reported wide success in the formation of stable radiolabeled complexes of drugs and nanocarriers and their use in pharmacokinetic studies (46–49). The drug and NPs were radiolabeled with ^{99m}Tc, and these radiolabeled complexes were intravenously administered to study blood clearance and biodistribution in mice model. Results of *in vivo* animal study showed clear advantage of PBCA-PEG20 over other formulations in terms of lower blood clearance, lower liver uptake, high blood concentration and prolonged plasma half life. Lower uptake in organs such as intestine and stomach confirmed *in vivo* stability of ^{99m}Tc-NP complex. *In vivo* results showed decrease in the concentration of PBCA NP in blood compartment with time and at the same time an increase in liver, showing increased PBCA NP uptakes by liver macrophage. In comparison to PBCA NP, PBCA-PEG20 NP showed longer residence in blood compartment and comparatively less uptake by liver, which displays its anti-phagocytic property. Tumor uptake was also found significantly high in the case of PBCA-PEG20 NP as a consequence of prolonged circulation resulting from more tumor retention by passive targeting through EPR effect. The ratio of blood to liver uptake results in *in-vivo* condition is also in compliance with *in vitro* phagocytic assay. The blood concentration of PBCA-PEG20 NP in blood remained significantly high even after 24 h in comparison to PBCA NP, which indicates long circulation half-life of PBCA-PEG20 NP.

CONCLUSION

The modified polymerization of BCA in presence of amine functional PEG has presented a promising approach to prepare PEGylated PBCA NP. These systems were also found useful as a drug delivery nanocarrier which gives high entrapment with desired particle size. The nanocarriers have displayed high colloidal stability in presence of strong aggregating agents such as sodium sulphate, calcium chloride and serum proteins. *In vitro* phagocytic studies also confirmed effectiveness of PEG coating in repelling phagocytic process. Various *in vitro* cell line studies demonstrated effectiveness of this carrier as a nanocarrier for drug delivery. *In vivo* biodistribution studies using ^{99m}Tc radiolabeling showed prolonged blood circulation half-life, less liver uptake and higher tumor retention property. Thus, it can be concluded that the PEGylated PBCA formulation can work as a novel tool for drug delivery which prevents RES uptake and prolongs circulation half life.

ACKNOWLEDGMENTS & DISCLOSURES

This research was supported by National Doctoral Fellowship by All India Council of Technical Education (AICTE) (1-10/RID/NDF-PG/(39)2008-2009), India. The authors are also thankful to Tong Shen Enterprise, Taiwan, for providing a free gift sample of n-butyl cyanoacrylate monomer.

REFERENCES

1. Nijhara R, Balakrishnan K. Bringing nanomedicines to market: regulatory challenges, opportunities, and uncertainties. Nanomedicine. 2006;2(2):127–36.
2. Koo OM, Rubinstein I, Onyuksel H. Role of nanotechnology in targeted drug delivery and imaging: a concise review. Nanomedicine. 2005;1(3):193–212.
3. Misra R, Acharya S, Sahoo SK. Cancer nanotechnology: application of nanotechnology in cancer therapy. Drug Discov Today. 2010;15(19–20):842–50.
4. Moghimi SM, Hunter AC, Murray JC. Long-circulating and target specific nanoparticles: theory to practice. Pharmacol Rev. 2001;53(2):283–318.
5. Mosqueira VCF, Legrand P, Gref R, Heurtault B, Appel M, Barratt G. Interactions between a macrophage cell line (J774A1) and surface-modified poly (D, L-lactide) nanocapsules bearing poly(ethylene glycol). J Drug Targeting. 1999;7(1):65–78.
6. Hans ML, Lowman AM. Biodegradable nanoparticles for drug delivery and targeting. Curr Opin Solid State Mater Sci. 2002;6(4):319–27.
7. Thiele L, Diederichs JE, Reszka R, Merkle HP, Walter E. Competitive adsorption of serum proteins at microparticles affects phagocytosis by dendritic cells. Biomaterials. 2003;24(8):1409–18.
8. Lacava LM, Lacava ZG, Da Silva MF, Silva O, Chaves SB, Azevedo RB, *et al.* Magnetic resonance of a dextran-coated magnetic fluid intravenously administered in mice. Biophys J. 2001;80(5):2483–6.
9. Strable E, Bulte JWM, Moskowitz B, Vivekanandan K, Allen M, Douglas T. Synthesis and characterization of soluble iron oxide −dendrimer composites. Chem Mater. 2001;13(6):2201–9.
10. Kohler N, Sun C, Fichtenholtz A, Gunn J, Fang C, Zhang MQ. Methotrexate-immobilized poly(ethylene glycol) magnetic nanoparticles for MR imaging and drug delivery. Small. 2006;2(6):785–92.
11. Quaglia F, Ostacolo L, De Rosa G, La Rotonda MI, Ammendola M, Nese G, *et al.* Nanoscopic core-shell drug carriers made of amphiphilic triblock and star-diblock copolymers. Int J Pharm. 2006;324(1):56–66.
12. Zahr AS, Davis CA, Pishko MV. Macrophage uptake of core-shell nanoparticles surface modified with poly(ethylene glycol). Langmuir. 2006;22(19):8178–85.
13. Liu L, Bai Y, Song C, Zhu D, Song L, Zhang H, *et al.* The impact of arginine-modified chitosan–DNA nanoparticles on the function of macrophages. J Nanopart Res. 2010;12(5):1637–44.
14. Pereverzeva E, Treschalin I, Bodyagin D, Maksimenko O, Kreuter J, Gelperina S. Intravenous tolerance of a nanoparticle-based formulation of doxorubicin in healthy rats. Toxicol Lett. 2008;178(1):9–19.
15. Gelperina SE, Khalansky AS, Skidan IN, Smirnova ZS, Bobruskin AI, Severin SE, *et al.* Toxicological studies of doxorubicin bound to polysorbate 80-coated poly(butyl cyanoacrylate) nanoparticles in healthy rats and rats with intracranial glioblastoma. Toxicol Lett. 2002;126(2):131–41.
16. Pereverzeva E, Treschalin I, Bodyagin D, Maksimenko O, Langer K, Dreis S, *et al.* Influence of the formulation on the tolerance profile of nanoparticle-bound doxorubicin in healthy rats: focus on cardio- and testicular toxicity. Int J Pharm. 2007;337(1–2):346–56.
17. Zhou Q, Sun X, Zeng L, Liu J, Zhang Z. A randomized multicenter phase II clinical trial of mitoxantrone-loaded nanoparticles in the treatment of 108 patients with unresected hepatocellular carcinoma. Nanomedicine. 2009;5(4):419–23.
18. Vauthier C, Dubernet C, Chauvierre C, Brigger I, Couvreur P. Drug delivery to resistant tumors: the potential of poly(alkyl cyanoacrylate) nanoparticles. J Controlled Release. 2003;93(2):151–60.
19. Couvreur P, Kante B, Roland M, Guiot P, Baudhuin P, Speiser P. Polycyanoacrylate nanocapsules as potential lysosomotropic carriers: preparation, morphological and sorptive properties. J Pharm Pharmacol. 1979;31(5):331–2.
20. Peracchia MT, Vauthier C, Puisieux F, Couvreur P. Development of sterically stabilized poly(isobutyl 2-cyanoacrylate) nanoparticles by chemical coupling of poly(ethylene glycol). J Biomed Mater Res Part A. 1997;34(3):317–26.
21. Peracchia MT, Vauthier C, Passirani C, Couvreur P, Labarre D. Complement consumption by poly(ethylene glycol) in different conformations chemically coupled to poly(isobutyl 2-cyanoacrylate) nanoparticles. Life Sci. 1997;61(7):749–61.
22. De Juan BS, Briesen HV, Gelperina SE, Kreuter J. Cytotoxicity of doxorubicin bound to poly(butyl cyanoacrylate) nanoparticles in rat glioma cell lines using different assays. J Drug Targeting. 2006;14(9):614–22.
23. Mitra A, Lin S. Effect of surfactant on fabrication and characterization of paclitaxel-loaded polybutylcyanoacrylate nanoparticulate delivery systems. J Pharm Pharmacol. 2003;55(7):895–902.
24. Eckelman WC. Radiolabeling with technetium-99m to study high-capacity and low-capacity biochemical systems. Eur J Nucl Med. 1995;22(3):249–63.
25. Babbar AK, Singh AK, Goel HC, Chauhan UPS, Sharma RK. Evaluation of 99mTc labeled Photosan-3, a heamatoporphyrin derivative, as a potential radiopharmaceutical for tumor scintigraphy. Nucl Med Biol. 2000;27(4):419–26.
26. Saha GB. Methods of radiolabeling. In: Saha GB, editor. Physics and radiobiology of nuclear medicine. New York: Springer; 1993. p. 100–6.
27. Saha GB. Fundamentals of nuclear pharmacy. 5th ed. New York: Springer; 2005.
28. Capala J, Barth RF, Bailey MQ, Fenstermaker RA, Marek MJ, Rhodes BA. Radiolabeling of epidermal growth factor with 99m Tc and *in vivo* localization following intracerebral injection into normal and glioma bearing rats. Bioconjugate Chem. 1997;8(3):289–95.
29. Mosmann T. Rapid colorimetric assay for cellular growth and survival: application to proliferation and cytotoxicity assays. J Immunol Methods. 1983;65(1–2):55–63.
30. Susin SA, Daugas E, Ravagnan L, Samejima K, Zamzami N, Loeffler M, *et al.* Two distinct pathways leading to nuclear apoptosis. J Exp Med. 2000;192(4):571–9.
31. Morse DL, Gray H, Payne CM, Gillies RJ. Docetaxel induces cell death through mitotic catastrophe in human breast cancer cells. Mol Cancer Ther. 2005;4(10):1495–504.
32. Behan N, Birkinshaw C, Clarke N. Poly n-butyl cyanoacrylate nanoparticles: a mechanistic study of polymerisation and particle formation. Biomaterials. 2001;22(11):1335–44.
33. Ryan B, McCann G. Novel sub-ceiling temperature rapid depolymerisation- repolymerisation reactions of cyanoacrylate polymers. Macromol Rapid Commun. 1996;17(4):217–27.

34. Limouzin C, Caviggia A, Ganachaud F, Hemery P. Anionic polymerization of n-butyl cyanoacrylate in emulsion and mini-emulsion. Macromolecules. 2003;36(3):667–74.
35. Huanga C, Chen C, Lee Y. Synthesis of high loading and encapsulation efficient paclitaxel-loaded poly(n-butylcyanoacrylate) nanoparticles via miniemulsion. Int J Pharm. 2007;338(1–2):267–75.
36. Pratten MK, Lioyd JB. Pinocytosis and phagocytosis: the effect of size of a particulate substrate on its mode of capture by rat peritoneal macrophages cultured *in vitro*. Biochim Biophys Acta. 1986;881(3):307–13.
37. Moghimi SM, Patel HM. Serum-mediated recognition of liposomes by phagocytic cells of the reticuloendothelial system: the concept of tissue specificity. Adv Drug Delivery Rev. 1998;32(1–2):45–60.
38. Blunk T, Hochstrasser DF, Sanchez JC, Muller BW, Muller RH. Colloidal carriers for intravenous drug targeting: plasma protein adsorption patterns on surface-modified latex particles evaluated by two-dimensional polyacrylamide gel electrophoresis. Electrophoresis. 1993;14(1):1382–7.
39. Muller M, Voros J, Csucs G, Walter E, Danuser G, Merkle HP, *et al.* Surface modification of PLGA microspheres. J Biomed Mater Res. 2003;66A(1):55–61.
40. Kanchan V, Panda AK. Interactions of antigen-loaded polylactide particles with macrophages and their correlation with the immune response. Biomaterials. 2007;28(35):5344–57.
41. Mühlfeld C, Rothen-Rutishauser B, Vanhecke D, Blank F, Gehr P, Ochs M. Visualization and quantitative analysis of nanoparticles in the respiratory tract by transmission electron microscopy. Part Fibre Toxicol. 2007;4:11.
42. Rothen-Rutishauser B, Mühlfeld C, Blank F, Musso C, Gehr P. Translocation of particles and inflammatory responses after exposure to fine particles and nanoparticles in an epithelial airway model. Part Fibre Toxicol. 2007;4:9.
43. Liu LX, Song CN, Song LP, Zhang HL, Dong X, Leng XG. Effects of alkylated-chitosan–DNA nanoparticles on the function of macrophages. J Mater Sci Mater Med. 2009;20(4):943–8.
44. Gref R, Domb A, Quellec P, Blunk T, Müller RH, Verbavatz JM, *et al.* The controlled intravenous delivery of drugs using PEG-coated sterically stabilized nanospheres. Adv Drug Delivery Rev. 1995;16(2–3):215–33.
45. Gref R, Quellec P, Marchand M, Dellacherie E, Lück M, Harnisch S, *et al.* "Stealth" corona-core nanoparticles surface modified by polyethylene glycol (PEG): influences of the corona (PEG chain length and surface density) and of the core composition on phagocytic uptake and plasma protein adsorption. Colloids Surf, B. 2000;18(3–4):301–13.
46. Arulsudar N, Subramanian N, Mishra P, Sharma RK, Murthy RSR. Preparation, characterization and biodistribution of 99mTc-labeled liposome encapsulated cyclosporine. J Drug Targeting. 2003;11(3):187–96.
47. Subramanian N, Arulsudar N, Chuttani K, Mishra P, Sharma RK, Murthy RSR. Radiolabeling, biodistribution and tumor imaging of stealth liposomes containing methotrexate. J Alasbimn. 2003;6(22):Article 6.
48. Arulsudar N, Subramanian N, Mishra P, Chuttani K, Sharma RK, Murthy RSR. Preparation, characterization and biodistribution of Technetium-99m-labeled leuprolide acetate-loaded liposomes in Ehrlich Ascites tumor bearing mice. AAPS PharmSci. 2004;6:E5.
49. Reddy LH, Sharma RK, Chuttani K, Mishra AK, Murthy RSR. Etoposide-incorporated tripalmitin nanoparticles with different surface charge: formulation, characterization, radiolabeling, and biodistribution studies. AAPS J. 2004;6(3):55–64.